NATIONAL ADVISORY COMMITTEE FOR AERONAUTICS

TECHNICAL NOTE 4166

AN EXPERIMENTAL AND THEORETICAL STUDY OF THE EFFECT OF FUEL ON PITCHING-TRANSLATION FLUTTER

By John L. Sewall

Langley Aeronautical Laboratory
Langley Field, Va.

Washington
December 1957

NATIONAL ADVISORY COMMITTEE FOR AERONAUTICS

TECHNICAL NOTE 4166

AN EXPERIMENTAL AND THEORETICAL STUDY OF THE EFFECT OF FUEL ON PITCHING-TRANSLATION FLUTTER

By John L. Sewall

SUMMARY

Analytical flutter studies were made for 2 two-dimensional fuel-loaded wing models, and the results are compared with experimental results for bending-to-torsion frequency ratios near 1. One of the models was made so that water, simulating fuel, could be carried internally in three compartments separated from each other by sealed spanwise partitions. The flutter speeds of this model for all fuel loads were highest for the compartmental-emptying sequence proceeding from front to rear. In the other model, fluid was carried externally in a geometrically scaled standard airplane fuel tank that was pylon mounted a distance of about $2\frac{1}{2}$ times the tank radius beneath the wing. Experimental results for this model have been reported in NACA Research Memorandum L55F10.

The results of flutter-speed calculations agreed well with experimental flutter speeds and flutter-speed trends when the analysis employed effective values for the mass and the mass moment of inertia together with theoretical slender-body air forces on the external tank and when the combined structural and fluid damping was considered to be zero. With the introduction of damping this agreement was improved for the internal-tank configuration and made worse for the external-tank configuration.

INTRODUCTION

The flutter of airplane wings with heavy fuel loads inherently involves the superposition and interaction of two highly complex dynamic phenomena, one associated with wing flutter and the other with fuel motion. This dual nature of the problem has motivated two main avenues of inquiry, one of which has been concerned with the fuel motion itself and the other with the effect of fuel motion on flutter. Fuel dynamic studies, such as references 1 to 6, have been chiefly concerned with finding ways to represent or approximate the complicated motion of the fuel in oscillating tanks.

Investigations of the effect of fuel motion on flutter have dealt with either realistic configurations, as, for example, in reference 7, or with simple models, as is the case in reference 8 and in the present paper. The purpose of using simple models for an investigation of this kind is to isolate as nearly as possible the effects of fuel motion in order to obtain results applicable to realistic configurations but not appreciably influenced by certain structural and aerodynamic effects peculiar to those configurations. With this purpose in mind, a two-dimensional wing apparatus was used in reference 8 to obtain flutter data for an external wing-tank configuration in which the tank was pylon mounted beneath a semirigid untapered wing mounted on bending and torsional springs located outside the airstream.

This same objective applies to the present paper which is primarily concerned with the correlation of flutter theory with experiment not only for some of the data presented in reference 8 but also for data obtained by using a two-dimensional internal wing-tank configuration. The two-dimensional features of the apparatus and models were particularly well suited to the simplest application of flutter theory because the assumption of two-dimensional air flow over the wing was more fully satisfied and because the structural behavior of the system could be adequately represented by just two vibration modes, namely, vertical translation (simulating first bending) and pitch (simulating first torsion). The mass and mass moment of inertia of the fuel were approximated by means of effective values which were determined during simple harmonic oscillations of the wing-tank system in vertical translation and pitch, respectively. As shown in references 4 to 6, these values are usually less than the mass and mass moment of inertia of the same volume of fuel at rest (or considered frozen). The results of reference 8 demonstrated the usefulness of references 4 to 6 by showing that, when the fluid in the tank was replaced by solid bodies having masses and mass moments of inertia equal to the corresponding effective values for the fluid, the model fluttered at the same speeds as it did with fluid. The present paper seeks to determine how well flutter speeds can be predicted by classical flexure-torsion theory based both on effective inertial properties of the fluid and on damping of the fluid according to a commonly used approximation.

The flutter analysis used is the same as that given in reference 9 except that the mass in translation is different from the mass in pitch. In addition, the aerodynamic forces on the external tank are included. The effect of these additional forces on flutter and divergence is explored for the external-tank model as a secondary objective of this paper. An appendix contains the flutter and divergence equations together with expressions for the tank aerodynamic coefficients derived by application of slender-body theory.

SYMBOLS

a	dimensionless distance of elastic axis relative to midchord, positive rearward
R	rearward fuel compartment of model A
b	semichord of wing, ft
C	center fuel compartment of model A
l_a	distance from wing quarter-chord to elastic axis, positive rearward, ft
l_T	distance from wing quarter-chord to volumetric centroid of external tank, positive rearward, ft
F	forward fuel compartment of model A unless otherwise noted
f	frequency, cps
f_h	uncoupled translation frequency, cps
f_α	uncoupled pitching frequency, cps
g	value of damping coefficient which satisfies flutter determinant as a function of $V/b\omega_\alpha$ in flutter analysis (see fig. 12)
g_h, g_α	experimentally determined damping coefficients in translation and pitch, respectively
h	vertical translation of elastic axis of wing section, or bending, positive down
$\bar{I}_\alpha$	mass moment of inertia of model in torsion about elastic axis, ft-lb-sec^2
$\bar{I}_{\alpha,F}$	effective mass moment of inertia of fluid about elastic axis, ft-lb-sec^2
$\bar{I}_{\alpha,S}$	mass moment of inertia of fluid considered as a solid about elastic axis, ft-lb-sec^2

$I_{T,\alpha}$ volume moment of inertia of external tank of model B about elastic axis, ft^5

k reduced frequency, $b\omega/V$

k_h spring constant of model in translation, lb/ft

k_α spring constant of model in pitch, ft-lb/radian

r outside radius of external tank of model B, ft

r_α dimensionless radius of gyration of model about elastic axis, $\sqrt{\bar{I}_\alpha / \bar{m}b^2}$

s wing semispan, ft

V airstream velocity, fps

$V_{f,0}$ experimental flutter speed of model in empty condition, used as a reference speed in figs. 6(b), 7(b), 8(b), 9, and 11, fps

v volume of external tank of model B, ft^3

$\bar{m}$ mass of model in torsion, $lb\text{-}sec^2/ft$

$\bar{m}'$ mass of model in bending, $lb\text{-}sec^2/ft$

$\bar{m}_F$ effective mass of fluid, $lb\text{-}sec^2/ft$

$\bar{m}_S$ actual mass of fluid (considered as a solid), $lb\text{-}sec^2/ft$

x_{ea} location of elastic axis of model from leading edge, percent chord (see table I)

x_{cg} location of model center of gravity from leading edge, percent chord (see table I)

x_α location of model center of gravity relative to semichord, measured from elastic axis, positive rearward

α angle of pitch of wing section about elastic axis, positive leading edge up

κ ratio of mass of cylinder of air of radius b to mass of model, $2\pi\rho b^2 s/\bar{m}$

ω angular frequency, radians/sec

ρ air density, lb-sec^2/ft^4

Subscripts:

d torsional divergence

f flutter

h translational degree of freedom

O tank-empty condition

T external tank of model B

α pitching degree of freedom

When used together the letters R, C, and F denote a particular fuel-emptying sequence for model A; for example, RCF identifies the sequence in which the rearward compartment is assumed to be emptied first, then the center compartment, and finally the forward compartment.

EXPERIMENTAL INVESTIGATION

Models and Apparatus

The experimental data presented in this paper were obtained by the use of two simplified wing models, cross-sectional views of which are shown in figure 1. One of these models, designated model A in figure 1(a), was made so that fluid could be carried internally in three compartments which were separated from each other by sealed spanwise partitions. In the other model, designated model B, the fluid was carried externally in a geometrically scaled standard airplane fuel tank that was pylon mounted a distance of about $2\frac{1}{2}$ times the tank radius beneath the wing as shown in figure 1(b). Both wings were of aluminum-alloy construction except for a wooden trailing edge on model A and an internal hardwood core formed to the airfoil contour of model B. The skin thickness for each model was 0.032 inch, and the thickness noted for model A in figure 1(a) includes a layer of fiber glass and Paraplex which was wrapped around the outside of the wing. The center of the tank pylon of model B was located above the center of the tank midsection and was fastened to the wing through a bracket which permitted chordwise variation of the center-of-gravity position of the pylon-tank assembly. Tables I and II list some additional data for the models.

Both models were fluttered in the same two-dimensional apparatus described in reference 8. A schematic view of this apparatus is shown in figure 2. Arrows indicate the translational and pitching degrees of freedom restrained by bending (translational) and torsional (pitching) springs which were mounted outside the test section of the Langley 2- by 4-foot flutter research tunnel.

The spring constants of one set of bending and torsional springs were selected so that the uncoupled-wing bending-to-torsion frequency ratios for both fuel-loaded models approached and exceeded 1 with increasing tank fullness. Values for the spring constants are given in table I. A second set of spring constants listed in the table for model B yielded frequency ratios greater than 1 for flutter conditions of this model without fuel over a range of forward and rearward center-of-gravity positions of the pylon-tank assembly from 30 to 60 percent wing chord.

Both models were fluttered in air at atmospheric pressure with fuel loads simulated by water and by solid weights. In model A the solid weights were mounted on the pitch axis outside the test section and in model B they were mounted inside the tank.

Effective Inertial Properties of Fuel-Loaded Wings

The apparatus was equipped with restraints so that the model could be excited in one degree of freedom independent of the other. This was an important feature because it permitted the measurement of uncoupled frequencies in either pure translation or pure pitch. These frequencies were used to determine the amount of fluid effective as mass and mass moment of inertia during flutter by application of essentially the same technique as that used in references 4 to 6. In order to determine the best approximations to effective values of these inertial properties at flutter, the frequencies read on the vibration records covered the same range of amplitudes encountered during flutter.

It is intended by repeated references to effective values to emphasize the fact that the effective mass and mass moment of inertia of an oscillating tank containing fluid are different from the mass and mass moment of inertia of the tank containing the same volume of fluid at rest, or in a solid condition. This behavior, of course, occurs because the fluid, during the oscillation, does not follow the motion of the tank perfectly. Indeed, as previously noted, references 4 to 6 have shown effective values of these properties to be generally less than the corresponding solid values, as might be intuitively expected.

The center-of-gravity variations with tank fullness are shown in figure 3. These variations are based on experimental values obtained with fluid in the tanks for the various fullnesses and fluid distributions

represented by the symbols. The straight lines connecting these symbols indicate that linear interpolation was employed to obtain centers of gravity for intermediate fullnesses and fluid distributions. For model A the symbol explanation in figure 3(a) applies throughout the paper and represents the fuel distribution in increments of full compartments for the six fuel-emptying sequences simulated in the experimental flutter program. In subsequent figures pertaining to model A the symbol explanation is modified to represent intermediate half-full compartments for which flutter tests were also conducted in the experimental program. Each sequence is represented by the order of the letters F, C, and R to indicate the order in which the compartments would be emptied during flight. For example, FCR applies to the sequence in which the forward compartment would be emptied first, then the center compartment, and finally the rearward compartment.

Figure 4 shows the variation of effective mass with tank fullness and figure 5, the variation of effective mass moment of inertia with tank fullness. The data in both figures have been referred to the mass and mass moment of inertia of the tank-empty condition for both models. Numerical values beside the points on the dotted curves and lines give the amount of fluid effective as mass and mass moment of inertia during translatory and pitching oscillations, respectively. In obtaining the data in figure 4, the variation of the measured translational frequency with mass was first established for several different solid weights mounted on each model in the empty condition. The effective mass of the model containing a given amount of fluid is, then, the empty mass plus the equivalent solid mass corresponding to the translational frequency measured for that fluid load. For model A the effective mass and actual mass were identical in all except the two fuel loadings indicated in figure 4(a).

The effective mass moments of inertia presented in figure 5(a) and table III were determined from the relation

$$\bar{I}_{\alpha} = \frac{k_{\alpha}}{(2\pi f_{\alpha})^2}$$

Values of $\bar{I}_{\alpha,F}/\bar{I}_{\alpha,S}$ greater than 1 cannot be readily explained but may be due to the swirling action of the fluid in a partly filled compartment. Moreover, where effective mass moments of inertia are only slightly greater than the mass moment of inertia of the empty model $\left(\text{that is, } \bar{I}_{\alpha}/\bar{I}_{\alpha,0} \approx 1\right)$, determination of the fluid-inertia ratio $\bar{I}_{\alpha,F}/\bar{I}_{\alpha,S}$ is subject to small-difference errors.

The method of determining the effective mass moments of inertia presented in figure 5(b) is similar to that used for the data in figure 4. Solid weights, mounted inside the empty external tank, were designed to the solid mass moments of inertia of the fuel for tank fullnesses up to 100 percent, and the variation of measured pitching frequency with these solid inertias was established. The effective mass moment of inertia of the model containing a given amount of fluid was then found by adding the model-empty mass moment of inertia to the equivalent solid mass moment of inertia corresponding to the measured pitching frequency for that fluid load.

Experimental Results

Model A.- As previously mentioned, the internal-tank configuration was tested with the wing filled with water in increments of half-full compartments for all six of the fuel-emptying sequences. Vibration and flutter data obtained in this program are given in table IV(a). The damping coefficients are based on logarithmic decrements of the amplitude decays for the natural frequencies listed in the table.

The damping coefficients and flutter speeds listed in table IV(a) are shown for the complete range of tank fullness in figures 6 to 8, in which the flutter speed is referred to the tank-empty flutter speed $V_{f,0}$. Figures 6(b), 7(b), and 8(b), together with figure 3(a), show that, except for the emptying of the center compartment in the RFC and FRC sequences (fig. 8(b)), the flutter speed consistently increased as the center of gravity was shifted rearward. If no attention is given to translation-to-pitch frequency ratios (equivalent to bending-to-torsion ratios), this trend appears at first glance to conflict with the established trend toward reduced flutter speed due to rearward center-of-gravity shifts for low frequency ratios. However, it has been shown in reference 10 that, when the frequency ratio lies within the range of 0.8 to about 1.3 for $a = -0.4$, $r_\alpha^2 = 0.25$, and $1/\kappa = 20$, the flutter speed experiences a marked increase as the center of gravity is moved back. This effect is similar to that found for the present configuration in which $a = -0.4$, r_α^2 ranged from 0.17 to 0.365, $1/\kappa$ ranged from 31 to 87, and for which the range of frequency ratio was from 0.76 to 1.06.

Further examination of the experimental flutter data in figures 6(b), 7(b), and 8(b) reveals the existence of an optimum fuel-emptying sequence, that is, the compartmental sequence resulting in the consistently highest flutter speeds for all fuel loads. This is the sequence which gives the most rearward center-of-gravity shift for any tank fullness and is designated FCR in figure 6(b), which also shows that the flutter speed for this sequence was as much as 22 percent higher than it was for the opposite sequence (RCF).

Model B.- The experimental results reported in the present paper supplement those reported in reference 8 for the unbaffled external-tank configuration. These results are listed in table IV(b). The damping coefficients for all partially full conditions were determined from frequency-response curves obtained at zero airspeed and correspond to the translational and pitching flutter amplitudes also listed in the table. The damping coefficients for the tank-empty and tank-full conditions were determined in the same manner as were those for model A.

The flutter speeds listed in table IV(b) are shown, referred to the tank-empty flutter speed, in figure 9 where they are given as functions of the tank fullness. Values of the frequency ratio ω_h/ω_α are shown beside each of the data points. The significance of these values with regard to fluid damping is discussed in reference 8 and in a subsequent section of the present paper. This strong frequency-ratio effect on flutter speed is not only of practical importance in realistic configurations but has also been encountered in such configurations as, for example, in the case of the dynamically scaled wing-tip tank model of reference 7.

The limiting effect of fluid turbulence on flutter amplitudes has also been discussed in reference 8 and is examined further in the present paper. As table IV(b) shows, the model fluttered over a wide speed range and a correspondingly limited amplitude range for all partially full conditions. Notice, however, that the flutter amplitudes consistently increased with further increase of speed for tank fullnesses ranging from 25 to 75 percent; whereas, for greater fullnesses the amplitudes tended to reach a peak and thereafter consistently decreased with increasing speed. This behavior may be seen more clearly in figure 10 in which the translational and pitching components of the flutter amplitudes are shown as functions of airstream velocity for the 85-, 90-, and 95-percent full conditions. Values of the damping coefficients g_h and g_α corresponding to the flutter amplitudes are shown beside each point. As noted in table IV(b) with the tank 95-percent full, the model essentially stopped fluttering when the pitching amplitude became 0° and the translational amplitude was barely visible. Thus, there appears to be a closed or bounded flutter-speed region for this case. On the basis of this experience and of the pitching-amplitude trends for the other two fuel loads, it was possible by extrapolation (indicated by the dashed curve) to establish closed flutter regions for these cases also. The upper flutter-speed boundary determined in this manner is shown in figure 9 in terms of the tank-empty flutter speed and can be seen to be anywhere from 62 to 97 percent higher than the lower flutter-speed boundary.

In addition to the fuel-load studies, flutter tests were also conducted for the empty external tank located at a few other chordwise center-of-gravity positions. A different set of bending and torsional springs was used, and the frequency ratios obtained were greater than 1. The results of these tests are given in table IV(c) and are shown as a function

of x_α in figure 11 in which the flutter speeds are referred to the same tank-empty flutter speed used for figure 9. The range of x_α values corresponds to a range of tank center-of-gravity positions from 30 percent wing chord to 60 percent wing chord. The damping coefficients are based on logarithmic decrements of the amplitude decays corresponding to the natural frequencies listed in the table. As was expected, the range of forward center-of-gravity positions at which flutter could be obtained was limited by the divergence-speed boundary.

ANALYTICAL INVESTIGATION

Method and Application of Analysis

The two-dimensional characteristics of the models and apparatus, as illustrated in figure 2, made the simplest form of flexure-torsion flutter theory, as given by the equations in the appendix, particularly applicable in the present paper. For one thing, the flutter mode could be adequately represented by just two degrees of freedom, namely, rigid vertical translation (equivalent to bending) and rigid pitch (equivalent to torsion). Moreover, the oscillatory aerodynamic forces and moments acting on the wing could be more truly reproduced by use of the classic incompressible-flow coefficients of reference 9.

The dynamic behavior of the fuel was represented in the flutter analysis by means of the effective values of mass and mass moment of inertia given in figures 4 and 5 and the measured damping coefficients given in table IV. The validity of using effective values for the inertial properties has been established experimentally in reference 8 wherein the flutter speeds of model B containing fluid were generally duplicated when the fluid was replaced by solid weights equivalent in effective mass and mass moment of inertia to the fluid. The measured damping coefficients were used to approximate the effect of damping at flutter by application of the well-known assumption given in reference 11, by which the damping coefficient g_h or g_α is considered to be indicative of the ability of a given configuration to change the flutter speed from that corresponding to $g = 0$, as may be seen, for example, in figure 12 which will be discussed later. The merits of this assumption are examined separately for each model.

Oscillating aerodynamic forces and moments acting on the external tank of model B were taken into account by application of the slender-body theory to obtain expressions from which aerodynamic coefficients for the tank were derived. As shown in the appendix, these coefficients were then simply added to the two-dimensional aerodynamic coefficients in the flutter analysis.

Analytical Results

The results of the analytical program are given in table V in the same order as the experimental results which are given in table IV. For model A, damping was introduced into the calculations according to the assumption specified in the preceding section, and the amount of damping assumed to be present was arbitrarily based on the larger value of damping coefficient listed for each fuel load in table IV(a). This predominant damping coefficient, either g_h or g_α, is repeated for each case in table V(a) and is plotted as a function of tank fullness and fuel distribution in figures 6(a), 7(a), and 8(a). The lower boundary of the shaded region in figures 6(b), 7(b), and 8(b) represents the calculated flutter speed with damping neglected, and the upper boundary represents the calculated flutter speed with damping included. As can be seen, the introduction of damping resulted in flutter-speed increases of from 1 to 14 percent.

The analytical results for model B are listed in tables V(b) and V(c). Since the tank was externally mounted, particular attention was directed to the effect of including oscillating aerodynamic forces and moments acting on the tank. The effect of damping is considered in the correlation of theory and experiment. For the fuel-loaded tank fixed at 40 percent wing chord, the linear superposition of two-dimensional wing forces and slender-body tank forces, according to the preceding section, reduced the flutter speed by 7 to 11 percent. For the tank-empty configuration, this reduction was increased from 7 percent for a frequency ratio of 0.67 to 10 percent for a frequency ratio of 1.13. When the empty tank was moved rearward to 60 percent of the wing chord, the inclusion of tank forces resulted in a reversed effect; that is, the flutter speed was increased by 10 percent for very nearly the same frequency ratio. (See also fig. 11.)

As a matter of interest, stimulated by the fact that model B without fuel encountered divergence rather than flutter with the tank center of gravity at 30 percent wing chord, the effect of tank aerodynamic forces on the divergence speed was examined by using the divergence-speed equation given in the appendix. The results are presented in table V(c) and are also shown in figure 11. As can be seen, the calculated divergence speeds obtained by including tank forces are approximately 10 percent lower than those obtained by neglecting tank forces.

CORRELATION OF THEORY AND EXPERIMENT

General Discussion

The experimental and analytical results of this investigation are compared in figures 6 to 8 for model A and in figures 9, 11, and 12 for

model B. As can be seen, the use of effective values of mass and mass moment of inertia in flutter calculations gave answers which agreed satisfactorily with experiment for nearly all fuel conditions. This result has also been obtained experimentally for model B in reference 8 which shows excellent agreement between the flutter speeds of the model with fluid and the flutter speeds of the model with solid weights equivalent in effective mass and effective mass moment of inertia to the fluid. For model A the calculated flutter speeds adequately follow the experimental trends for all fuel-emptying sequences and are consistently conservative, or less than the experimental flutter speeds, by margins ranging from 2 to 20 percent. When fluid damping was taken into account in the manner previously described, these margins narrowed to less than 10 percent, and the calculated flutter speeds were still conservative.

Neglect of aerodynamic forces and moments on the external tank of model B led to calculated flutter speeds that were as much as 11 percent unconservative, or greater than the experimental flutter speeds, for the fuel-loaded configuration. (See fig. 9 for the 25-percent-full condition.) With tank forces included, the calculations became generally conservative. As can be seen, theory appears to follow closely the experimental trend up to the 95-percent-full condition for which the calculated flutter speed was infinite, whereas the experimental flutter speed was not.

Calculated flutter speeds were also conservative for model B in the empty condition with the tank center of gravity located at various chordwise positions ranging from 30 percent wing chord to 60 percent wing chord. As is shown in figure 11, the difference between calculated and experimental flutter speed amounts to as much as 21 percent. Furthermore, theory including tank aerodynamic forces exhibits a somewhat more consistent tendency to parallel experiment than does theory neglecting tank forces. It can also be noted that inclusion of tank forces resulted in a calculated divergence speed which agreed well with the experimental divergence speed for the tank at 30 percent wing chord but was 6 percent less than the experimental flutter speed when the tank was at 40 percent wing chord.

Some Further Remarks on Damping

The improved agreement between theory and experiment due to considering g equal to the experimental value of g_h or g_α, whichever is larger, has already been discussed for model A. For model B, however, the situation is different. Figure 12 shows g as a function of flutter-speed coefficient $V/b\omega_\alpha$ for all the tank fullnesses tested with model B. The solid curves define theoretical borderline conditions between stable and unstable motion over a limited range of g. In order to be consistent with the assumption regarding damping, the experimental flutter results from table IV(b) are positioned in figure 12 according to experimental

values of g_h and g_α. The points identified by the open circles represent speeds at which the borderline conditions between stable and unstable motion were first encountered experimentally. The solid circles represent experimental flutter speeds within the unstable region for all partially full conditions in which the flutter amplitudes were limited by fluid turbulence. The theoretical solutions at $g = 0$ correspond to the calculated flutter-speed ratios presented in figure 9 with tank aerodynamic forces and moments included. The relation between theory and experiment for the tank-empty configuration (fig. 12(a)) is similar to that found for all cases for model A.

It is important to note that the effect of damping appears to be more pronounced at the higher fuel loads as is indicated by the consistent decrease in the slope of the theoretical curve. This behavior is attributed primarily to the fact that the frequency ratio approached and exceeded 1 as the tank fullness approached 100 percent. The dashed line shown in figure 12(g) represents the stable condition (i.e., no flutter) shown in figure 10 for a torsional component of the flutter amplitude equal to zero.

This sensitivity of theory to small amounts of damping was also typical of the cases of the empty-tank configuration tested with the tank in different chordwise positions. Inclusion of damping according to the assumption $g = g_h$, where g_h is less than g_α, resulted in flutter speeds that were unconservative by as much as 78 percent with the tank center of gravity at 40 percent wing chord.

CONCLUSIONS

This paper reports experimental and analytical investigations of flutter of two simplified fuel-loaded wing configurations, the two-dimensional characteristics of which are particularly suited to the simplest application of classical flexure-torsion flutter theory. The wings of both models were semirigid, untapered, and mounted on bending and torsional springs located outside the airstream. Water was used to simulate fuel carried internally in one configuration in three compartments separated from each other by sealed spanwise partitions and carried externally in the other configuration in a geometrically scaled, pylon-mounted, standard airplane fuel tank. The results of the investigations appear to justify the following conclusions for these configurations:

1. For the wing with fuel stored in compartments within the wing structure and with bending-to-torsion frequency ratios ranging from 0.76 to 1.06, optimum (i.e., consistently highest) flutter speeds were found

for the compartmental-emptying sequence proceeding from front to rear and corresponding to the most rearward shift in the center of gravity. It should be noted that this trend is in contrast to the established trend toward reduced flutter speeds due to rearward center-of-gravity shifts for low frequency ratios.

2. The conclusion of NACA Research Memorandum L55F10 is herein reaffirmed, namely, that effective or average values of mass and mass moment of inertia should be used in flutter calculations of fuel-loaded wings.

3. For the external wing-tank configuration the inclusion of slender-body approximations to the aerodynamic forces and moments acting on the external tank at flutter tended to improve the agreement between flutter theory and experiment.

4. Arbitrarily assuming the damping coefficient at flutter to be either the coefficient in translation or pitch gave conservative answers that agreed well with experiment for the internal-tank configuration but, for the wing with the external fuel tank, flutter speeds calculated on the basis of either damping coefficient were unconservative by wide margins.

Langley Aeronautical Laboratory,
National Advisory Committee for Aeronautics,
Langley Field, Va., August 20, 1957.

APPENDIX

FLUTTER AND DIVERGENCE EQUATIONS FOR TWO-DIMENSIONAL WING-TANK CONFIGURATION

Flutter

The calculated flutter speeds presented in the body of this paper were obtained by use of the equations given in this appendix. As previously noted, the aerodynamic forces and moments acting on the external wing-tank configuration of model B were approximated by a simple linear superposition of two-dimensional and slender-body aerodynamic theories. The two-dimensional forces for the wing are those given in reference 9, and the slender-body forces acting on the external tank are essentially the same as those given in reference 12 for closed bodies of revolution. The fineness ratio of the external tank of model B, namely 7.13 (see table I), is, as shown in reference 13, within the range of fineness ratio for which the basic slender-body assumption of two-dimensional incompressible flow in planes normal to the free-stream direction is applicable.

Linearly superposing wing and tank aerodynamic forces and moments by simply adding them together results in the following equations of motion:

$$-\bar{m}'\omega^2 h + k_h\left(1 + ig_h\right)h - \bar{m}bx_\alpha\omega^2\alpha - \left(\bar{P} + P_T\right) = 0 \tag{1}$$

$$-\bar{m}bx_\alpha\omega^2 h + k_\alpha\left(1 + ig_\alpha\right)\alpha - \bar{I}_\alpha\omega^2\alpha - \left(\bar{M}_\alpha + M_{\alpha,T}\right) = 0 \tag{2}$$

in which the mass in translation $\bar{m}'$ is greater than the mass in pitch $\bar{m}$ because it includes the torsional springs (see fig. 2) and where

$$P_T = \rho v\omega^2 h - \rho v\omega^2\alpha\left(l_a - l_T + i\,\frac{b}{k}\right)$$

$$M_{\alpha,T} = \rho v\omega^2 h\left(l_T - l_a + i\,\frac{b}{k}\right) + \rho\omega^2\alpha\left(I_{T,\alpha} + \frac{b^2}{k^2}v\right)$$

$$v = \int_{Tank} \pi r^2 dx \qquad \bar{m}' = \int_{Span} m' dy$$

$$l_T = \frac{1}{v} \int_{Tank} \pi x r^2 dx \qquad \bar{m} = \int_{Span} m \, dy$$

$$I_{T,\alpha} = \int_{Tank} \pi (x - l_a)^2 r^2 dx \qquad \bar{I}_\alpha = \int_{Span} I_\alpha \, dy$$

$$\bar{P} = \int_{Span} P \, dy$$

$$\bar{M}_\alpha = \int_{Span} M_\alpha \, dy$$

In these equations, x is the chordwise coordinate measured from the wing quarter-chord, positive rearward; y is the spanwise coordinate; m' is the mass of the model in translation per unit span; m is the mass of the model in pitch per unit span; I_α is the mass moment of inertia of the model in pitch about the elastic axis, per unit span; P is the aerodynamic force acting on the wing per unit span; and M_α is the aerodynamic moment acting on the wing about the elastic axis per unit span. The foregoing integrals for the tank were evaluated numerically over the tank length on the basis of the tank ordinates given in table II, and the results are given in table II(b) for all tank positions considered in the body of the paper.

Introducing uncoupled frequencies by means of the expressions $\omega_h^2 = k_h/\bar{m}'$ and $\omega_\alpha^2 = k_\alpha/\bar{I}_\alpha$ and performing certain algebraic manipulations leads to the equilibrium equations

$$\frac{h}{b} A_{11} + \alpha B_{11} = 0 \tag{3}$$

$$\frac{h}{b} D_{11} + \alpha E_{11} = 0 \tag{4}$$

from which is obtained the determinantal flutter equation

$$\begin{vmatrix} A_{11} & B_{11} \\ D_{11} & E_{11} \end{vmatrix} = 0 \tag{5}$$

where

$$A_{11} = \left[1 - \left(\frac{\omega_h}{\omega}\right)^2\left(1 + ig_h\right)\right]\frac{1}{\kappa'} - \left(A_{ch} + A_{ch,T}\right)$$

$$B_{11} = \frac{x_\alpha'}{\kappa'} - \left(A_{c\alpha} + A_{c\alpha,T}\right)$$

$$D_{11} = \frac{x_\alpha}{\kappa} - \left(A_{ah} + A_{ah,T}\right)$$

$$E_{11} = \left[1 - \left(\frac{\omega_\alpha}{\omega}\right)^2\left(1 + ig_\alpha\right)\right]\frac{r_\alpha^2}{\kappa} - \left(A_{a\alpha} + A_{a\alpha,T}\right)$$

$$x_\alpha' = \frac{\bar{m}}{\bar{m}'}x_\alpha \qquad \kappa' = \frac{2\pi\rho b^2 s}{\bar{m}'} \qquad \kappa = \frac{2\pi\rho b^2 s}{\bar{m}} \qquad r_\alpha^2 = \frac{\bar{I}_\alpha}{\bar{m}b^2}$$

The aerodynamic coefficients for the wing, from reference 14, are

$$A_{ch} = -1 - \frac{2G}{k} + i\frac{2F}{k}$$

$$A_{c\alpha} = a + \frac{2F}{k^2} - \left(\frac{1}{2} - a\right)\frac{2G}{k} + i\left[\frac{1}{k} + \frac{2G}{k^2} + \left(\frac{1}{2} - a\right)\frac{2F}{k}\right]$$

$$A_{ah} = -\frac{1}{2} - \left(\frac{1}{2} + a\right)A_{ch}$$

$$A_{a\alpha} = -\frac{1}{8} - a^2 - \left(\frac{1}{2} + a\right)\frac{2F}{k^2} + \left(\frac{1}{4} - a^2\right)\frac{2G}{k} +$$

$$i\left[\left(\frac{1}{2} - a\right)\frac{1}{k} - \left(\frac{1}{4} - a^2\right)\frac{2F}{k} - \left(\frac{1}{2} + a\right)\frac{2G}{k^2}\right]$$

where F and G are the well-known aerodynamic functions derived in reference 9, and the aerodynamic coefficients for the tank are

$$A_{ch,T} = -\frac{v}{2\pi b^2 s}$$

$$A_{c\alpha,T} = -A_{ch,T}\left(\frac{l_a - l_T}{b} + i\,\frac{1}{k}\right)$$

$$A_{ah,T} = A_{ch,T}\left(\frac{l_T - l_a}{b} + i\,\frac{1}{k}\right)$$

$$A_{a\alpha,T} = -\frac{I_{T,\alpha}}{2\pi b^4 s} + A_{ch,T}\,\frac{1}{k^2}$$

Divergence

Since torsional divergence is a static instability associated with the torsional degree of freedom, the speed at which an external wing-tank configuration will diverge can be obtained by setting $h = 0$ (eq. (1)) and $\omega = 0$, whence $F + iG \rightarrow 1$. Under these conditions the divergence speed v_d, which can be obtained from a reduced form of equation (2), is given by

$$\frac{v_d}{b\omega_\alpha} = \sqrt{\frac{r_\alpha^2}{k}\,\frac{1}{2\left(a + \frac{1}{2}\right) - A_{ch,T}}} \tag{6}$$

The divergence speeds presented in the main body of this paper were calculated by means of this equation.

REFERENCES

1. Graham, E. W.: The Forces Produced by Fuel Oscillation in a Rectangular Tank. Rep. No. SM-13748, Douglas Aircraft Co., Inc., Apr. 13, 1950.

2. Lorell, Jack: Forces Produced by Fuel Oscillations. Progress Rep. No. 20-149 (Contract No. DA-04-495-Ord 18), C.I.T., Jet Propulsion Lab., Oct. 16, 1951.

3. Graham, E. W., and Rodriguez, A. M.: The Characteristics of Fuel Motion Which Affect Airplane Dynamics. Rep. No. SM-14212, Douglas Aircraft Co., Inc., Nov. 27, 1951.

4. Merten, Kenneth F., and Stephanson, Bertrand H.: Some Dynamic Effects of Fuel Motion in Simplified Model Tip Tanks on Suddenly Excited Bending Oscillations. NACA TN 2789, 1952.

5. Widmayer, Edward, Jr., and Reese, James R.: Moment of Inertia and Damping of Fluid in Tanks Undergoing Pitching Oscillations. NACA RM L53E01a, 1953.

6. Reese, James R., and Sewall, John L.: Effective Moment of Inertia of Fluid in Offset, Inclined, and Swept-Wing Tanks Undergoing Pitching Oscillations. NACA TN 3353, 1955.

7. Gayman, William H.: An Investigation of the Effect of a Varying Tip Weight Distribution on the Flutter Characteristics of a Straight Wing. Jour. Aero. Sci., vol. 19, no. 5, May 1952, pp. 289-301.

8. Reese, James R.: Some Effects of Fluid in Pylon-Mounted Tanks on Flutter. NACA RM L55F10, 1955.

9. Theodorsen, Theodore: General Theory of Aerodynamic Instability and the Mechanism of Flutter. NACA Rep. 496, 1935.

10. Theodorsen, Theodore, and Garrick, I. E.: Mechanism of Flutter - A Theoretical and Experimental Investigation of the Flutter Problem. NACA Rep. 685, 1940.

11. Smilg, Benjamin, and Wasserman, Lee S.: Application of Three-Dimensional Flutter Theory to Aircraft Structures. ACTR No. 4798, Materiel Div., Army Air Corps, July 9, 1942.

12. Clevenson, S. A., Widmayer, E., Jr., and Diederich, Franklin W.: An Exploratory Investigation of Some Types of Aeroelastic Instability of Open and Closed Bodies of Revolution Mounted on Slender Struts. NACA TN 3308, 1954. (Supersedes NACA RM L53E07.)

13. Ashley, H., Zartarian, G., and Neilson, D. O.: Investigation of Certain Unsteady Aerodynamic Effects in Longitudinal Dynamic Stability. USAF Tech. Rep. No. 5986 (Contract No. AF 33(038)-11668, RDO No. R458-414b), Wright Air Dev. Center, U.S. Air Force, M.I.T., Dec. 1951.

14. Barmby, J. G., Cunningham, H. J., and Garrick, I. E.: Study of Effects of Sweep on the Flutter of Cantilever Wings. NACA Rep. 1014, 1951. (Supersedes NACA TN 2121.)

TABLE I.- PERTINENT MODEL CHARACTERISTICS

	Model A	Model B
b, ft	0.5	0.5
2s, ft	2	2
Airfoil section	NACA 65-010	NACA 65-010
Fineness ratio of external tank	----------	7.13
Maximum fuel length (chordwise), in.:		
Forward compartment	2.205	----------
Center compartment	3.33	----------
Rearward compartment	4.55	----------
Maximum fuel depth, in.:		
Forward compartment	0.92	----------
Center compartment	1.12	----------
Rearward compartment	1.05	----------
Midsection	----------	4.19
Maximum external diameter of tank, in.	----------	4.25
x_{ea}, percent chord	30.0	40.0
x_{cg}, percent chord:		
All tanks empty	43.5	43.9
Forward tank full	36.4	----------
Rearward tank full	52.0	----------
All tanks full	42.8	39.5
k_h, lb/ft	1,955 ----------	2,015 3,340
k_α, ft-lb/radian	83.6 ----------	343.5 204.1
$\bar{m}'$, lb-sec^2/ft:		
All tanks empty	0.294	0.404
All tanks full	0.497	0.712
$\bar{m}$, lb-sec^2/ft:		
All tanks empty	0.1203	0.2285
All tanks full	0.323	0.536
$\bar{I}_\alpha$, ft-lb-sec^2:		
All tanks empty	0.00862	0.0309
All tanks full (solid)	0.0209	0.1805
f_h, cps:		
All tanks empty	13.0	11.2
All tanks full	9.97	8.36
f_α, cps:		
All tanks empty	15.8	16.7
All tanks full	10.35	7.22
$g_{h,0}$	0.013	0.009
$g_{\alpha,0}$	0.025	0.018

TABLE II.- GEOMETRIC PROPERTIES OF EXTERNAL TANK OF MODEL B

(a) Tank ordinates

Distance from nose of tank, in.	r, ft
0	0
1.09	.0658
2.03	.1016
3.41	.1358
4.54	.1542
5.88	.1684
8.58	.1750
9.875	.1770
18.33	.1770
20.47	.1716
23.77	.1275
27.18	.0642
30.3	0

(b) Volumetric properties

Tank center of gravity, percent chord	l_T, ft	v, ft	$I_{T,\alpha}$, ft^5
30	0.01584	0.05415 × π	0.01662 × π
40	.1158	.05415	.01570
50	.2160	.05415	.01586
60	.3160	.05415	.01714

TABLE III.- MASS MOMENT-OF-INERTIA DATA FOR MODEL A

Emptying sequence	Fullness, percent	Distribution			Ratios of mass moments of inertia		
		F	C	R	$\bar{I}_\alpha/\bar{I}_{\alpha,0}$		$\frac{\bar{I}_{\alpha,F}}{\bar{I}_{\alpha,S}}$
					Effective	Solid	
FCR	100				2.300	2.423	0.91
	91				2.232	2.352	.91
	83				2.155	2.280	.90
	61				2.155	2.231	.94
	39				2.106	2.181	.94
	20				1.614	1.591	1.04
	0				1.000	1.000	-----
CRF	78				2.300	2.373	0.95
	56				2.271	2.324	.96
	37				1.739	1.733	1.01
	17				1.140	1.143	.98
	8.6				1.072	1.071	1.01
RFC	80.5				1.845	1.832	1.02
	61				1.217	1.242	.90
	52				1.159	1.170	.94
	44				1.092	1.099	.93
	22				1.063	1.049	1.28
FRC	63				1.735	1.690	1.065
CFR	47.5				2.203	2.252	0.96
RCF	39				1.188	1.192	0.98

TABLE IV.- EXPERIMENTAL RESULTS

(a) Model A

Emptying sequence	Fullness, percent	Distribution			Frequencies			Damping coefficients		ρ, lb-sec^2/ft^4	V_f, fps	$\frac{1}{k}$
		F	C	R	f_h, cps	f_α, cps	f_f, cps	g_h	g_α			
FCR	100				9.97	10.35	10.4	0.009	0.0235	0.002363	139	4.25
	91				10.1	10.5	10.5	.016	.0195	.002360	147	4.46
	83				10.3	10.7	10.8	.010	.022	.002371	153	4.51
	61				10.95	10.7	11.35	.031	.025	.002405	155	4.35
	39				11.45	10.8	11.9	.012	.025	.002395	159	4.25
	20				12.2	12.3	13.4	.0285	.054	.002354	146	3.47
	0				13.0	15.8	14.4	.013	.025	.002438	[a]135	2.98
CRF	78				10.4	10.35	10.8	0.024	0.021	0.002421	142	4.185
	56				10.95	10.4	11.2	.009	.021	.002423	143	4.06
	37				11.6	11.9	12.4	.025	.059	.002436	125	3.21
	17				12.3	14.7	13.0	.010	.022	.002464	118	2.89
	8.6				12.6	15.15	14.0	.017	.030	.002573	129	2.95
RFC	80.5				10.35	11.5	11.0	0.018	0.0315	0.002469	126	3.65
	61				10.9	14.2	11.9	.010	.024	.002473	134	3.58
	32				11.1	14.6	12.2	.055	.028	.002451	137	3.57
	44				11.4	15.0	12.6	.011	.022	.002455	141	3.56
	22				12.3	15.15	14.0	.056	.0245	.002461	157	3.115
FRC	65				10.8	11.9	11.9	0.019	0.054	0.002438	141	3.77
CFR	47.5				11.2	10.6	11.3	0.0155	0.022	0.002426	153	4.31
RCF	39				11.5	14.4	12.7	0.029	0.0265	0.002481	130	3.26

[a]Reference flutter speed $V_{f,0}$ (see figs. 6(b), 7(b), and 8(b)).

TABLE IV.- EXPERIMENTAL RESULTS - Continued

(b) Model B - Fuel-loaded configuration

$[k_h = 2{,}015$ lb/ft; $k_\alpha = 343.5$ ft-lb/radian$]$

Fullness, percent	Frequencies			Flutter amplitudes		Damping coefficients		ρ, lb-sec^2/ft^4	V_f, fps	$\frac{1}{k}$
	f_h, cps	f_α, cps	f_f, cps	Translation, in.	Pitch, deg	g_h	g_α			
0	11.2	16.7	12.9	----	----	0.009	0.018	0.002448	[b]217	5.36
25	10.35	13.7	11.4	0.19	0.9	0.029	0.072	0.002461	178	4.97
			11.4	.20	1.0	.0295	.073	.002461	181	5.06
			11.3	.23	1.3	.0305	.077	.002457	188	5.30
			11.4	.29	1.5	.034	.080	.002458	191	5.335
50	9.64	11.4	10.2	0.24	2.0	0.027	0.078	0.002465	152	4.74
			10.2	.30	2.1	.030	.079	.002462	161	5.025
			10.2	.33	2.3	.0345	.082	.002465	168	5.24
75	9.06	10.1	9.21	0.27	2.0	0.027	0.074	0.002475	132	4.56
			9.21	.33	2.1	.032	.0745	.002472	141	4.88
			9.21	.38	2.2	.039	.0755	.002471	148	5.12
85	8.70	9.43	8.91	0.135	0.8	0.026	0.060	0.002525	120	4.29
			8.77	.235	1.1	.026	.0615	.002526	129	4.68
			8.77	.255	1.0	.026	.061	.002520	133	4.83
			8.78	.27	.95	.026	.061	.002519	143	5.18
			8.72	.32	.8	.029	.060	.002513	159	5.805
			8.65	.29	.65	.027	.060	.002509	174	6.405
90	8.62	9.09	8.82	0.10	0.55	0.026	0.050	0.002519	119	4.295
			8.78	.12	.6	.026	.050	.002518	125	4.53
			8.64	.145	.45	.026	.050	.002514	143	5.27
			8.62	.15	.4	.026	.0495	.002509	160	5.91
			8.55	.15	.3	.026	.049	.002503	176	6.56
			8.57	.14	.2	.026	.0485	.002494	202	7.505
95	8.45	8.26	8.54	0.06	0.25	0.026	0.038	0.002519	101	3.765
			8.57	.09	.3	.026	.038	.002514	129	4.79
			8.55	.06	.15	.026	.038	.002510	143	5.325
			[c]8.40	.02	0	.026	.0375	.002506	164	6.22
			[c]8.33	.02	0	.026	.0375	.002497	191	7.30
100	8.36	7.22	-----	----	----	0.027	0.026	0.002393	[d]324	-----

[b]Reference flutter speed $V_{f,0}$ (see figs. 9 and 11).

[c]Bending frequencies, flutter not discernible from oscillograph records.

[d]Maximum tunnel airspeed, no flutter.

TABLE IV.- EXPERIMENTAL RESULTS - Concluded

(c) Model B - Effect of tank center of gravity on tank-empty configuration

$\left[k_h = 3{,}340 \text{ lb/ft}; k_\alpha = 204.1 \text{ ft-lb/radian}\right]$

Tank center-of-gravity position, percent wing chord	x_α	Frequencies			Damping coefficients		ρ, lb-sec^2/ft^4	V_f, fps	$\frac{1}{k}$
		f_h, cps	f_α, cps	f_f, cps	g_h	g_α			
30	0.0233	14.2	12.4	----	0.008	0.020	0.002378	[e]275	----
40	.0767	14.2	12.6	13.7	.009	.022	.002284	295	6.87
50	.128	14.1	12.4	13.3	.013	.021	.002315	233	5.56
60	.182	14.1	12.15	13.0	.008	.022	.002404	236	5.78

[e]Divergence (based on $q = 90$ lb/ft^2 and standard conditions), no flutter.

TABLE V.- ANALYTICAL RESULTS

(a) Model A

Emptying sequence	Fullness, percent	Distribution			Without damping			With damping ($g = g_h$ or g_α)				
		F	C	R	V_f, fps	f_f, cps	$\frac{1}{k}$	g_h	g_α	V_f, fps	f_f, cps	$\frac{1}{k}$
FCR	100				123	10.8	3.63	-----	0.0235	127	10.6	3.83
	91				133	10.9	3.89	-----	.0195	136	10.7	4.05
	83				142	11.0	4.11	-----	.022	145	10.8	4.27
	61				148	11.6	4.04	0.031	------	149	11.3	4.18
	39				144	12.3	3.73	-----	.025	147	11.9	3.95
	20				127	13.3	3.05	-----	.054	140	12.7	3.50
	0				125	14.3	2.775	-----	.025	128	14.2	2.89
CRF	78				127	11.0	3.66	0.024	-----	131	10.8	3.85
	56				126	11.6	3.46	-----	0.021	131	11.3	3.69
	37				104	12.5	2.66	-----	.059	118	12.0	3.13
	17				109	13.1	2.64	-----	.022	113	13.1	2.75
	8.6				118	13.7	2.74	-----	.030	123	13.55	2.89
RFC	80.5				110	11.2	3.15	-----	0.0515	117	10.9	3.40
	61				122.5	11.7	3.33	-----	.024	127	11.7	3.44
	52				127	12.0	3.36	0.033	-----	131	12.0	3.47
	44				139	12.7	3.47	-----	.022	141	12.65	3.55
	22				125	13.6	2.94	.036	-----	130	13.4	3.10
FRC	63				126	11.7	3.42	-----	0.054	132	11.4	3.67
CFR	47.5				136	11.9	3.64	-----	0.022	139	11.7	3.77
RCF	39				115.5	12.3	2.98	0.029	-----	122	12.3	3.14

TABLE V.- ANALYTICAL RESULTS - Concluded

(b) Model B - Effect of including aerodynamic forces on external tank containing fuel

Fullness, percent	Without tank aerodynamic forces			With tank aerodynamic forces		
	V_f, fps	f_f, cps	$\frac{1}{k}$	V_f, fps	f_f, cps	$\frac{1}{k}$
0	223	13.0	5.46	209	13.1	5.05
25	198	11.45	5.50	182	11.4	5.07
50	163	10.5	4.94	152	10.6	4.57
75	129.5	9.63	4.28	121.5	9.60	4.03
85	120	8.80	4.34	112	9.07	3.92
90	104	8.85	3.74	94	8.87	3.36
95						
100						

(c) Model B - Effect of tank position on flutter and divergence of tank-empty configuration

$$\left[\frac{\bar{m}}{\bar{m}_0} = 1.023\right]$$

Tank center-of-gravity position, percent wing chord	x_α	$\frac{\bar{I}_\alpha}{\bar{I}_{\alpha,0}}$	Without tank aerodynamic forces				With tank aerodynamic forces			
			V_d, fps	V_f, fps	f_f, cps	$\frac{1}{k}$	V_d, fps	V_f, fps	f_f, cps	$\frac{1}{k}$
30	0.0233	1.019	292				269			
40	.0767	1.019	305	269	13.6	6.30	278	244	13.5	5.75
50	.128	1.040	300	196	13.4	4.65	274.5	198	13.5	4.67
60	.182	1.070	294	183	13.5	4.32	268	202	13.4	4.80

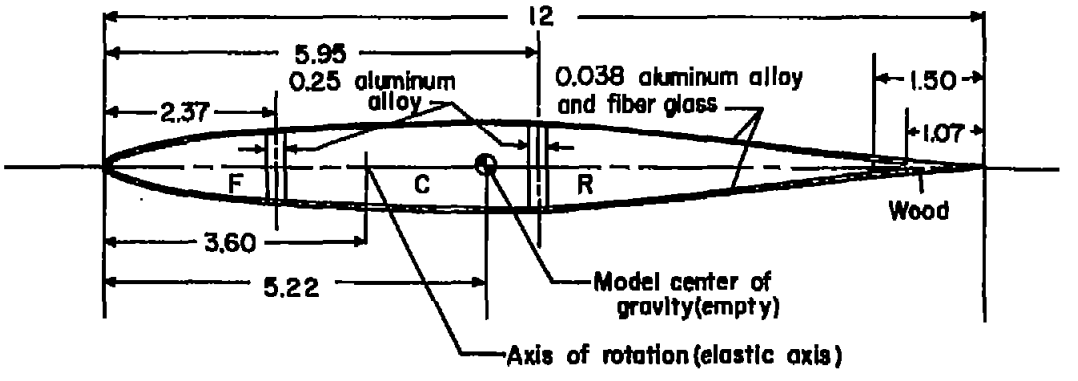

(a) Model A.

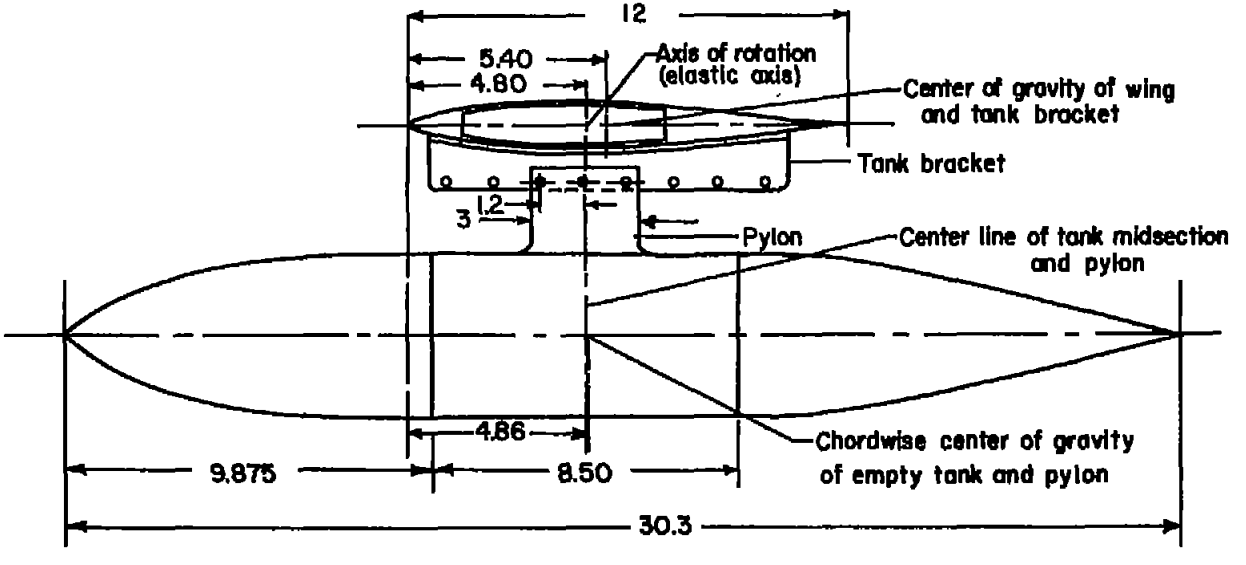

(b) Model B.

Figure 1.- Cross-sectional views of flutter models. All dimensions shown are in inches.

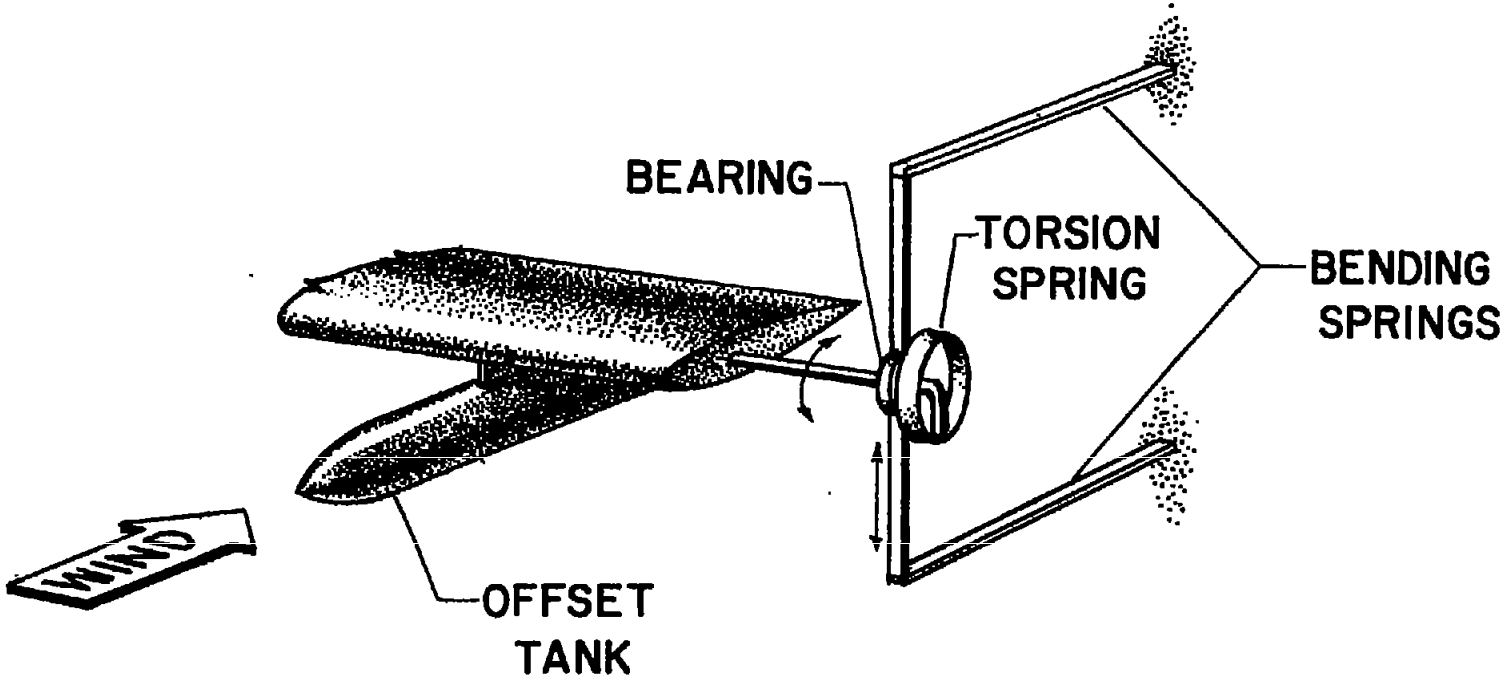

Figure 2.- Schematic view of flutter model B and apparatus (fig. 2 of ref. 8).

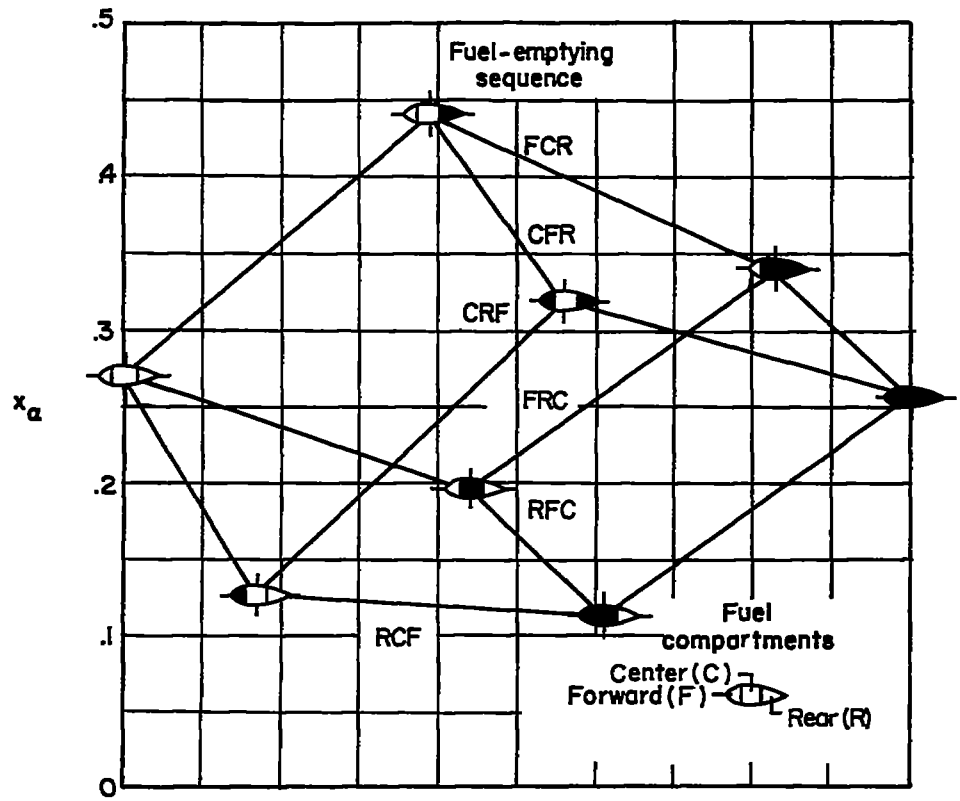

(a) Model A.

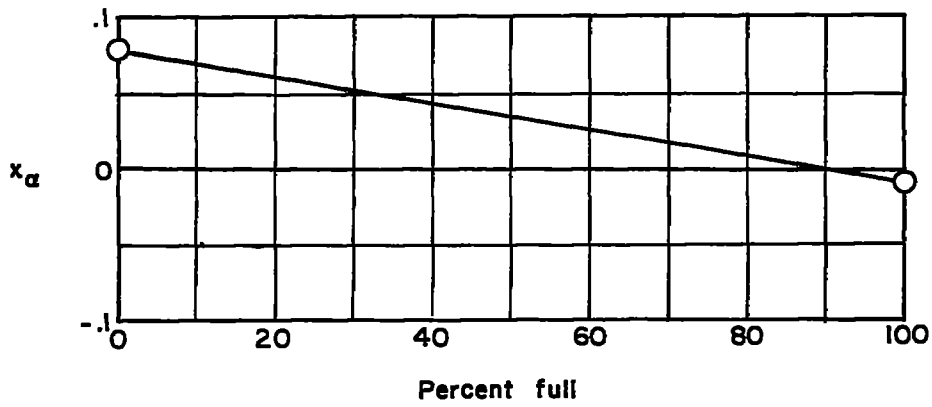

(b) Model B.

Figure 3.- Center-of-gravity variations for fuel-loaded wings. Symbols indicate measured values.

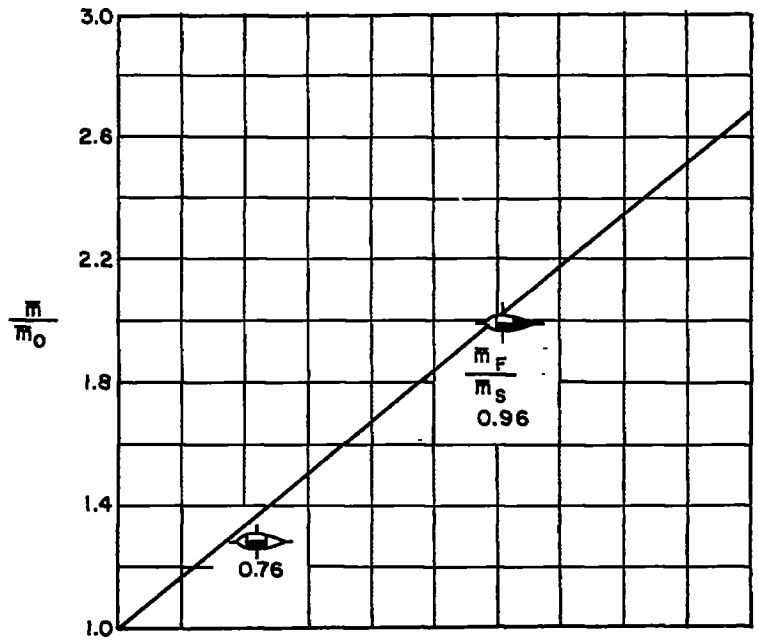

(a) Model A.

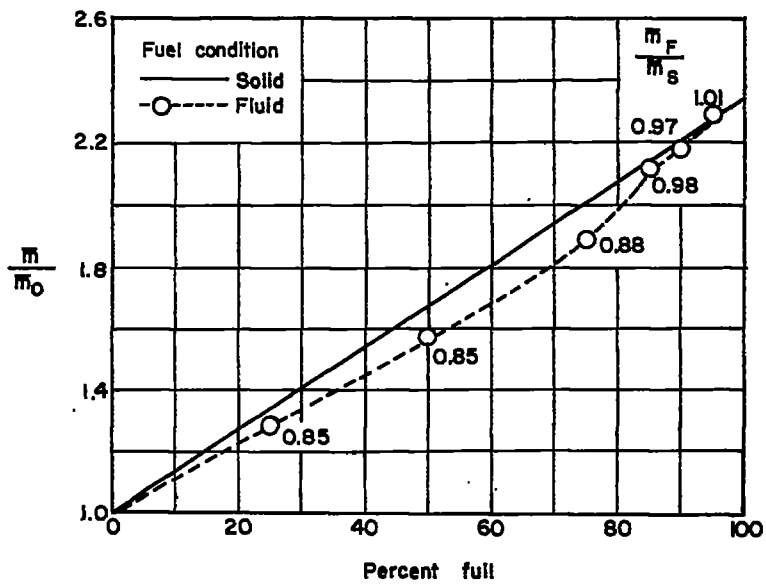

(b) Model B.

Figure 4.- Mass variations for fuel-loaded wings.

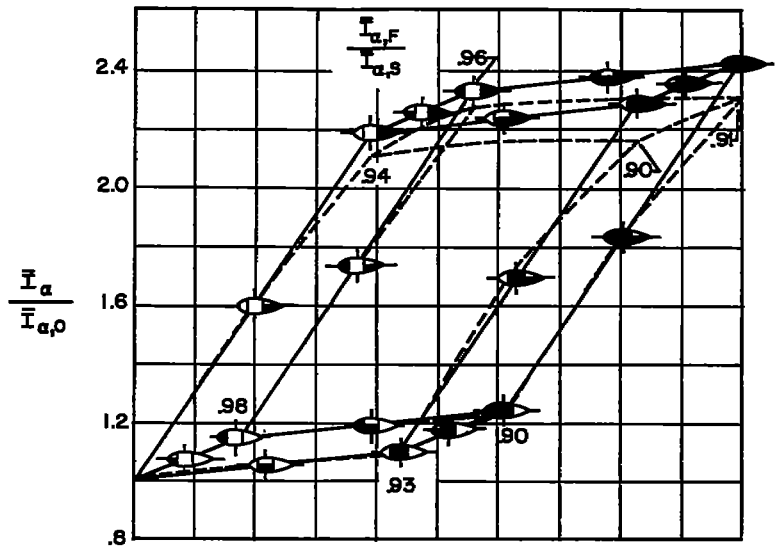

(a) Model A.

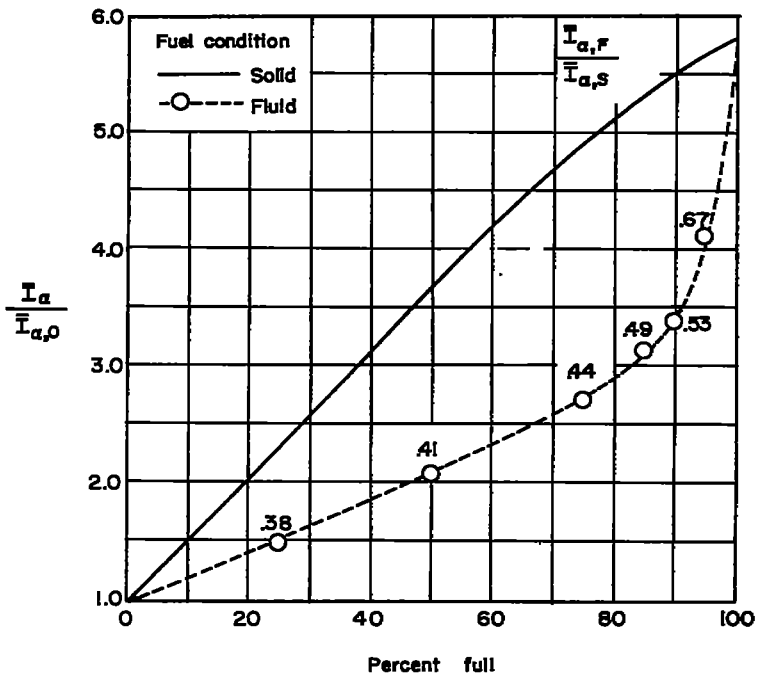

(b) Model B.

Figure 5.- Variations in mass moment of inertia about elastic axis for fuel-loaded wings.

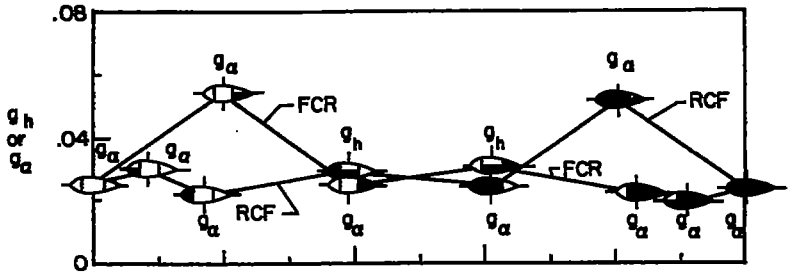

(a) Predominant damping coefficients.

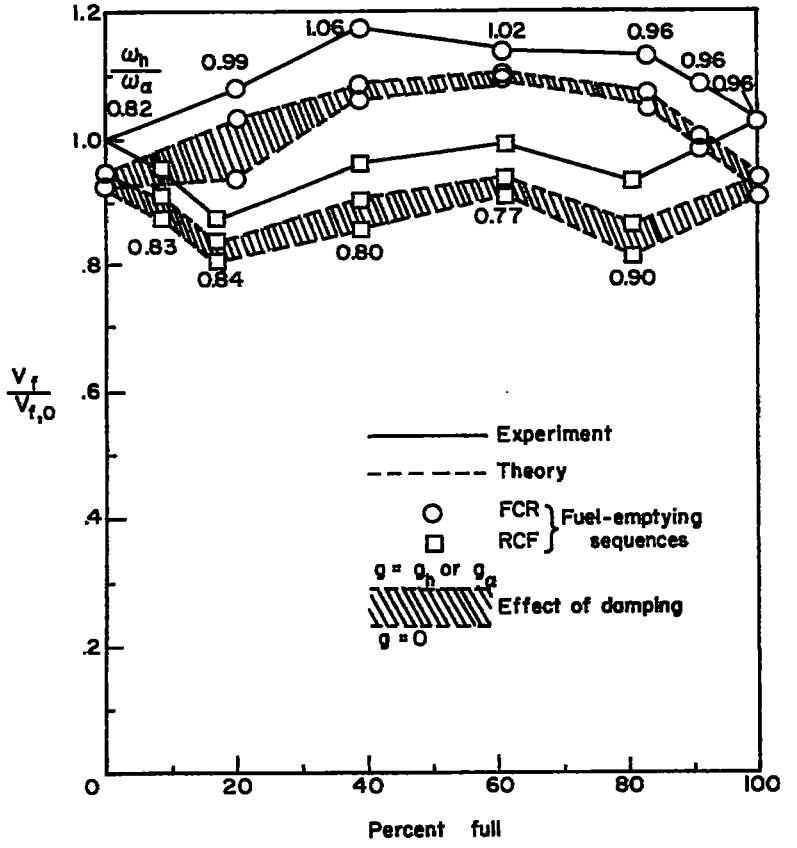

(b) Flutter speed ratios.

Figure 6.- Comparison of experimental and calculated flutter speeds, including effect of damping, for fuel-emptying sequences FCR and RCF of model A.

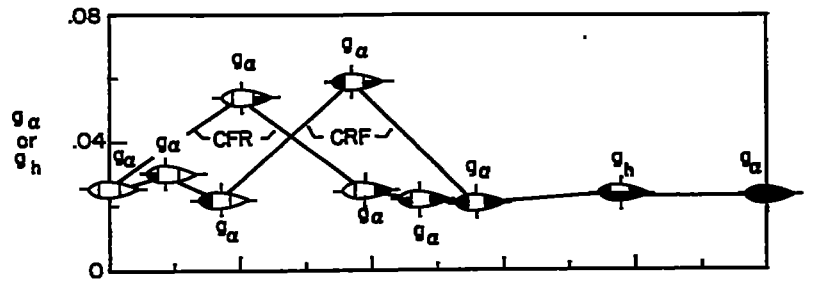

(a) Predominant damping coefficients.

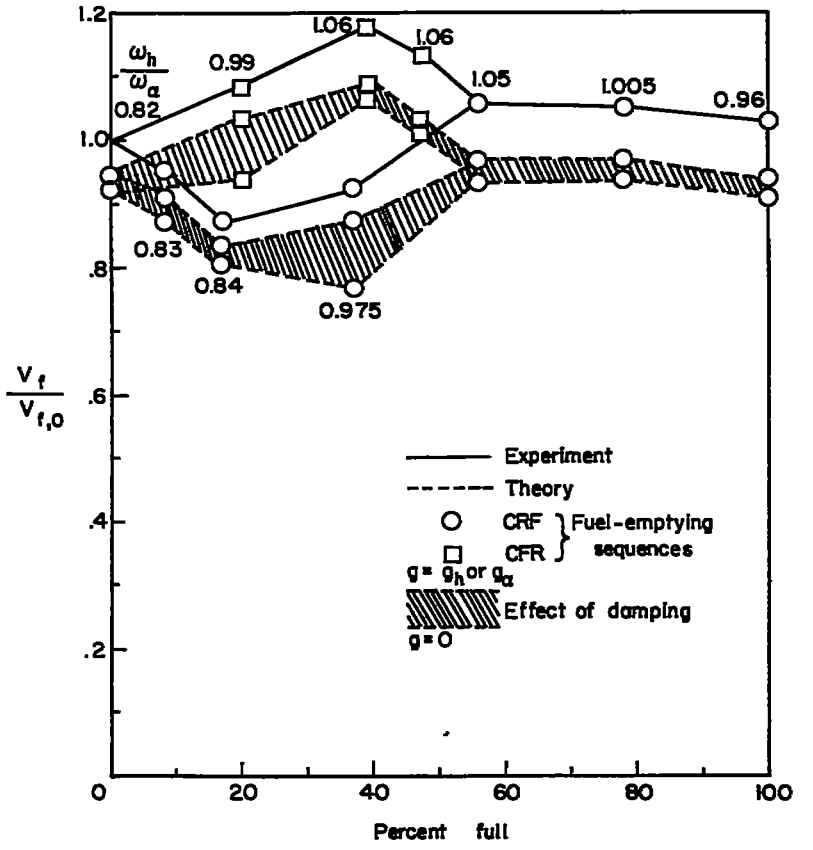

(b) Flutter speed ratios.

Figure 7.- Comparison of experimental and calculated flutter speeds, including effect of damping, for fuel-emptying sequences CRF and CFR of model A.

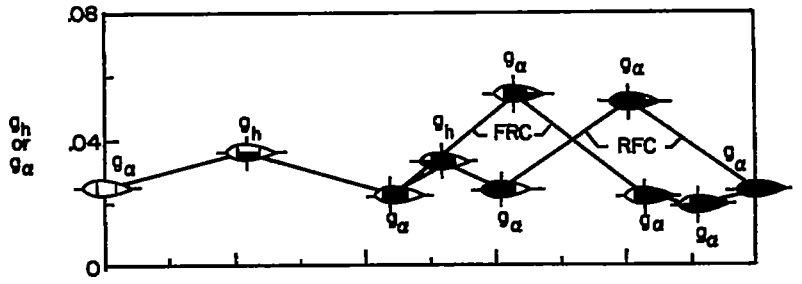

(a) Predominant damping coefficients.

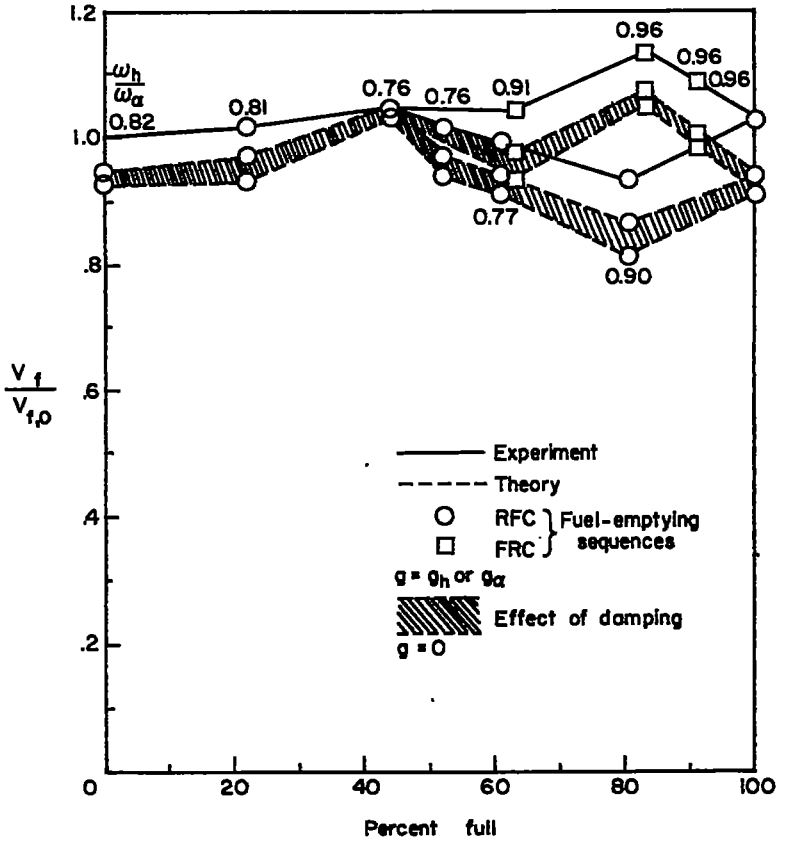

(b) Flutter speed ratios.

Figure 8.- Comparison of experimental and calculated flutter speeds, including effect of damping, for fuel-emptying sequences RFC and FRC of model A.

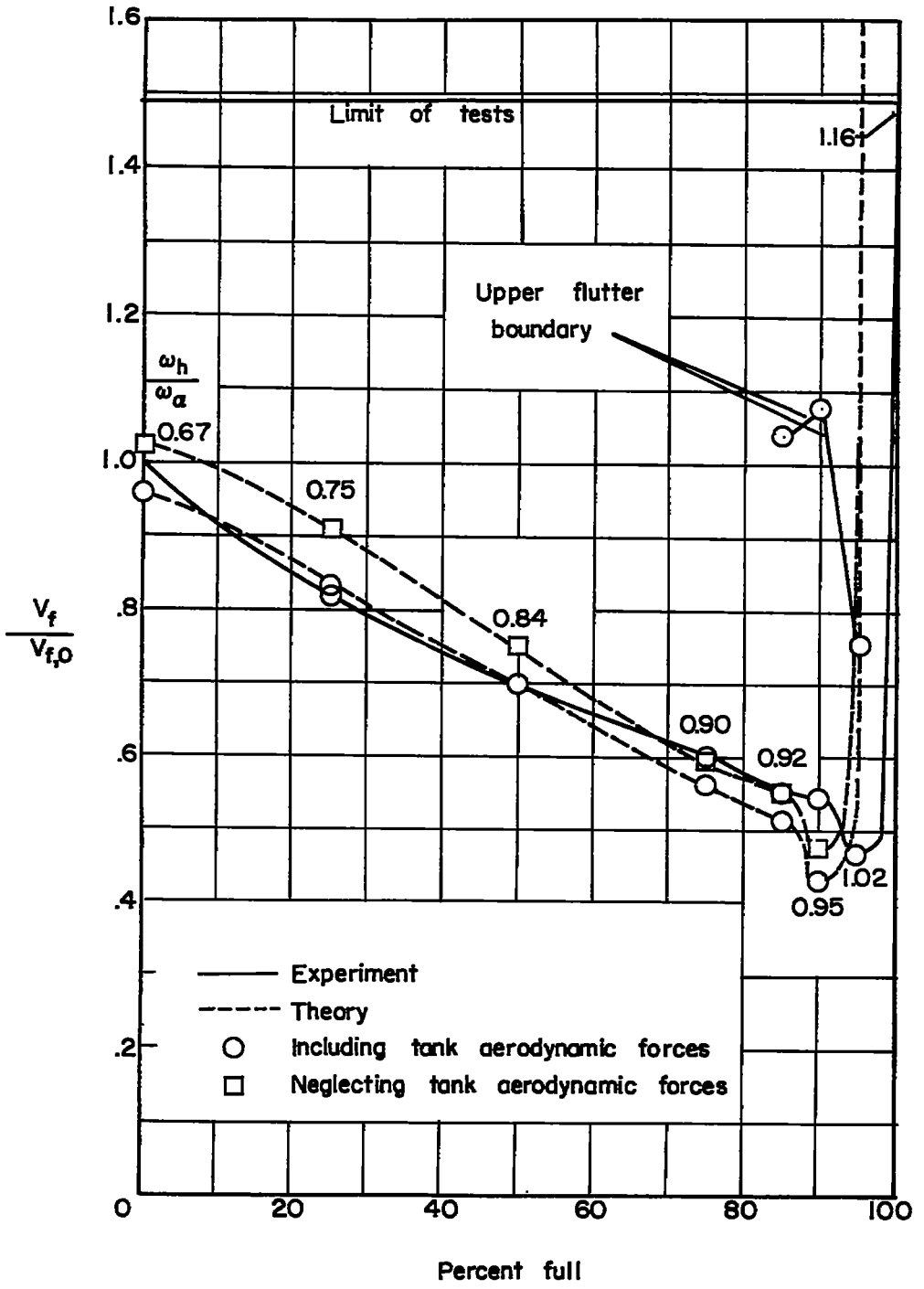

Figure 9.- Comparison of experimental and calculated flutter speeds for model B with fuel.

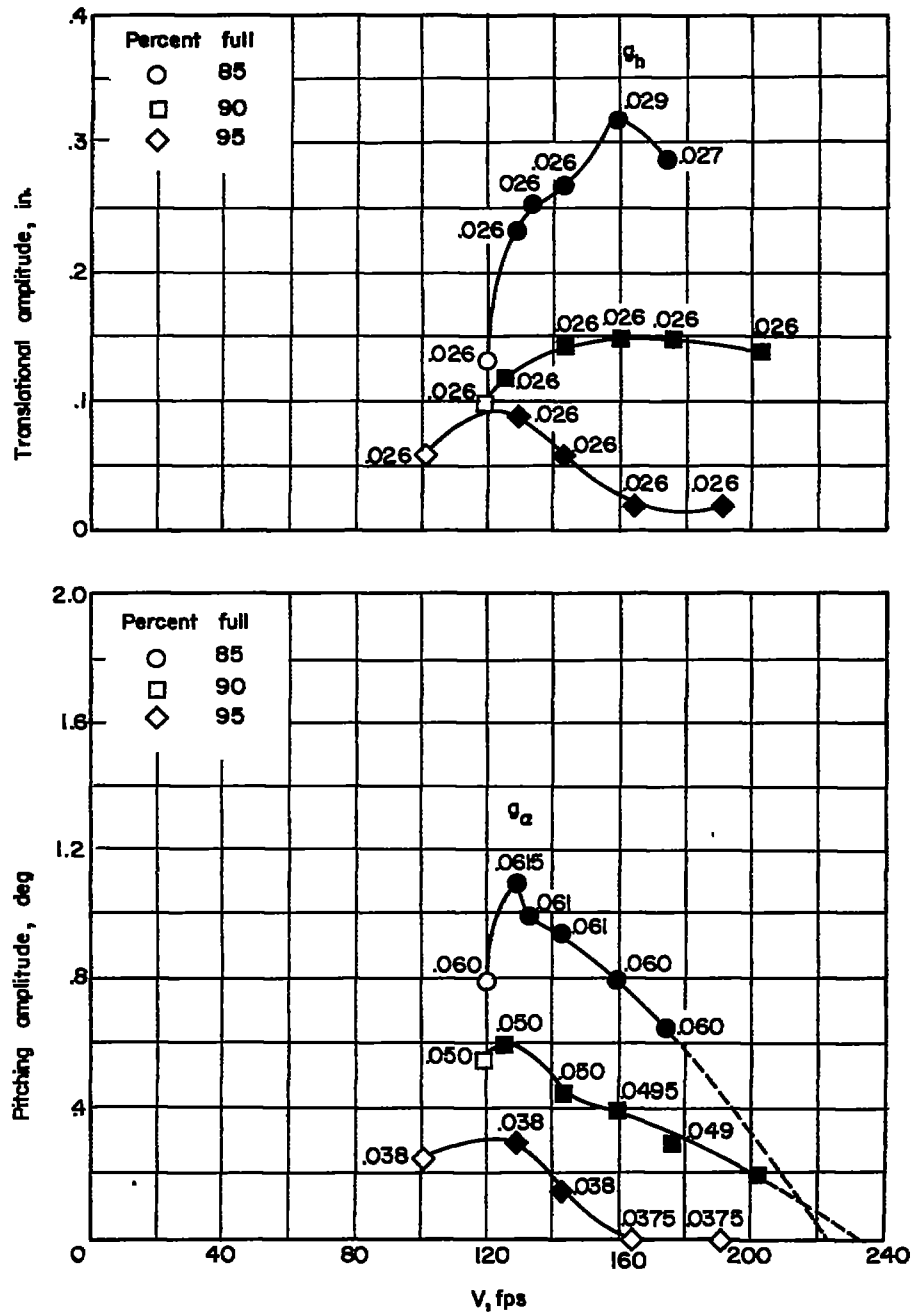

Figure 10.- Effect of fluid on flutter amplitudes of model B without baffles. The dashed curves indicate extrapolations. Open symbols denote initial flutter points and solid symbols denote limited-amplitude flutter.

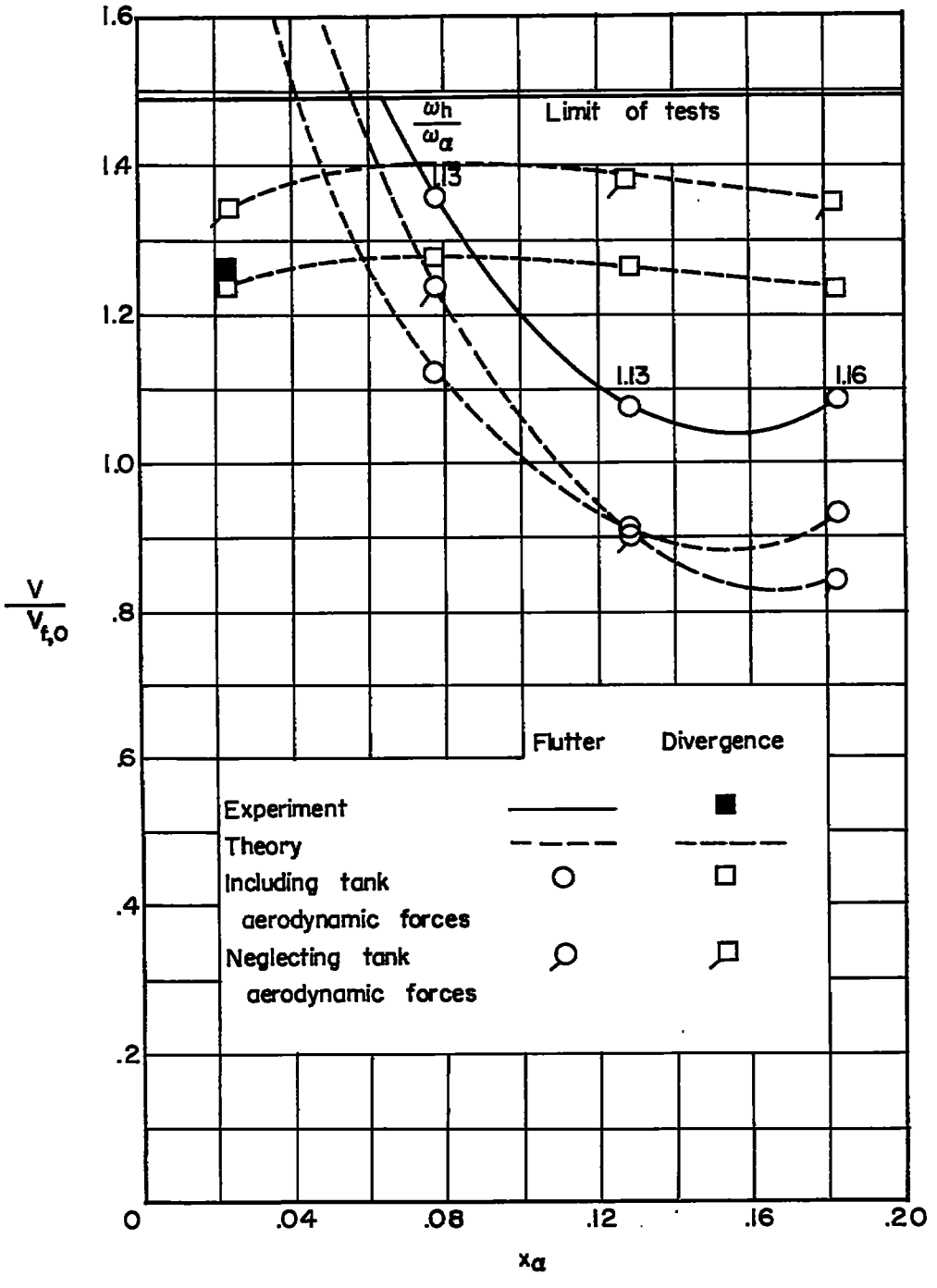

Figure 11.- Comparison of experimental and calculated flutter and divergence speeds for model B without fuel.

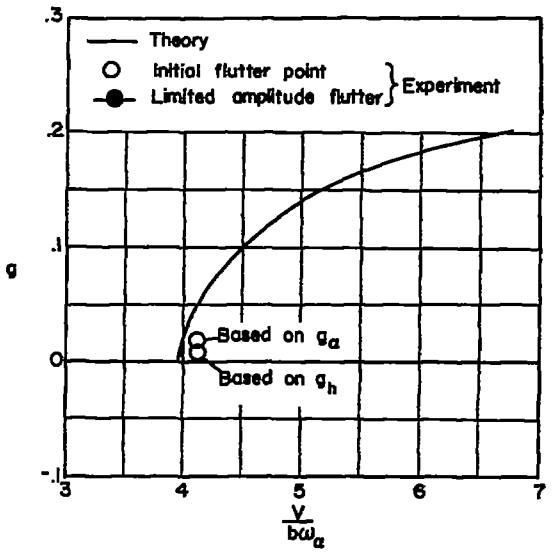

(a) Tank empty; $\frac{\omega_h}{\omega_\alpha} = 0.67$.

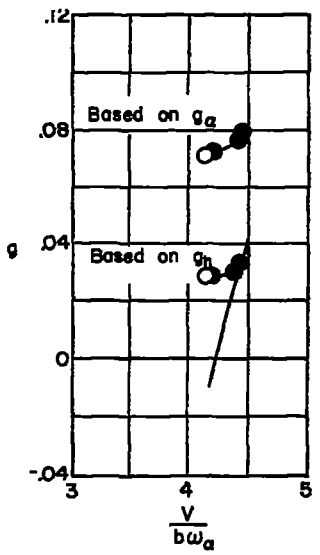

(b) 25 percent full; $\frac{\omega_h}{\omega_\alpha} = 0.75$.

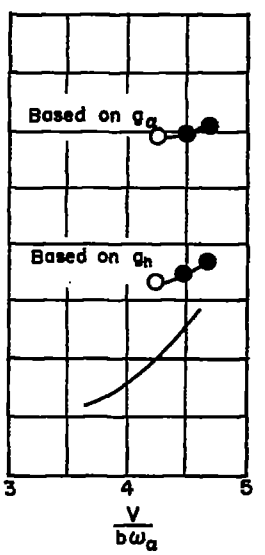

(c) 50 percent full; $\frac{\omega_h}{\omega_\alpha} = 0.84$.

Figure 12.- Correlation of theoretical flutter solutions with experiment, including damping and aerodynamic tank forces, for model B.

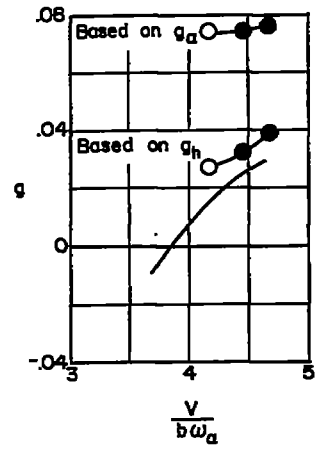

(d) 75 percent full; $\frac{\omega_h}{\omega_\alpha} = 0.90$.

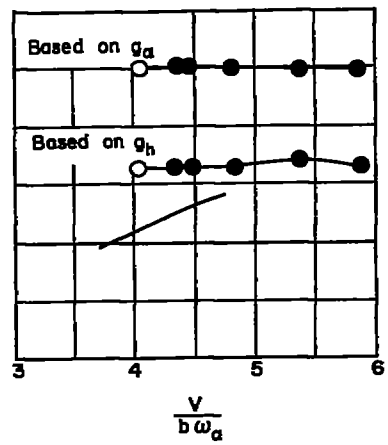

(e) 85 percent full; $\frac{\omega_h}{\omega_\alpha} = 0.92$.

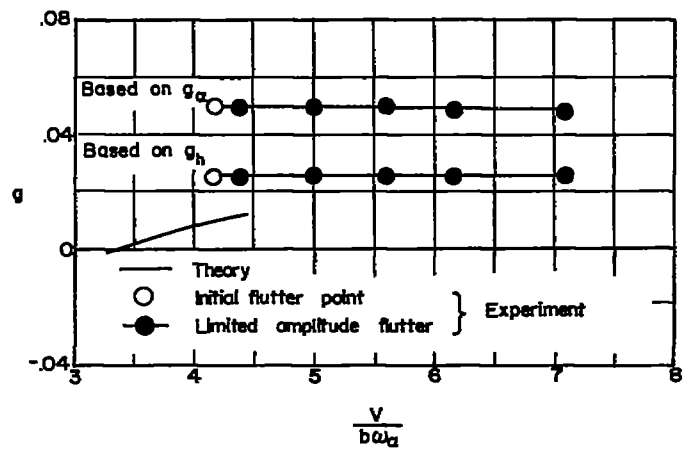

(f) 90 percent full; $\frac{\omega_h}{\omega_\alpha} = 0.95$.

Figure 12.- Continued.

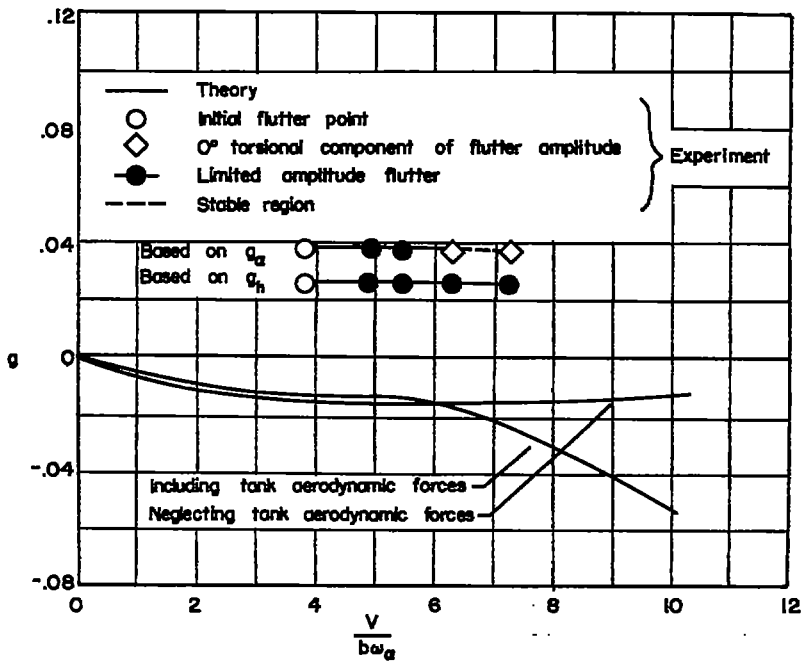

(g) 95 percent full; $\frac{\omega_h}{\omega_\alpha} = 1.02$.

Figure 12.- Concluded.